Surface Science 176 (1986) 295–318
North-Holland, Amsterdam

PHASE DIAGRAMS FOR H/Ni(111) BASED ON MODEL INTERACTIONS: EFFECTS OF STRONG LONG-RANGE ATTRACTIONS

L.D. ROELOFS *, T.L. EINSTEIN, N.C. BARTELT and J.D. SHORE *

Department of Physics and Astronomy, University of Maryland, College Park, MD 20742, USA

Received 20 February 1986; accepted for publication 7 May 1986

We test the pairwise adatom–adatom interaction sets for H/Ni(111) computed by Muscat by using Monte Carlo techniques to determine the lattice gas phase diagrams they imply and then comparing with experiment. Although the correct ordered phase is reproduced and the maximum disordering temperature is approximately correct, there remain topological discrepancies with the experimental phase diagram. The origin of the main discrepancy is a relatively strong long-range attractive interaction. We describe the behavior this interaction causes and outline the circumstances under which similar phenomena might occur in other systems, developing insight through (re-)examination of the square-lattice Ising metamagnet problem. Finally we show how two previously studied interaction sets with relatively weak sixth-neighbor attractions lead to more accurate phase diagrams. One appendix collects some results on the metamagnet. Two others present transfer matrix scaling calculations of the critical properties of the disordering of two ordered states on a honeycomb lattice: hard hexagons (nearest neighbor exclusion) is Ising-like to high precision, while graphitic (2×2) is 4-state-Potts-like.

1. Introduction

During the last decade, considerable progress has been achieved in the calculation of the interactions between chemisorbed atoms on transition metal surfaces. Early efforts, aimed at understanding qualitative trends, simplified this complicated problem by treating either only substrate d-bands (typically via tight-binding) or the s-electrons (with jellium) [1]. With the recognition that both contribute substantially to the adsorption energy has come a search for ways to include both aspects in a computationally tractable scheme. Muscat and Newns [2–4], have approached this problem by embedding in jellium several spheres containing atomic potentials; the $l = 2$ phase shifts then give an account of d-band effects. Other efforts have been carried out with (1) effective medium theory [5] (which Muscat [4,6–9] has also used recently to replace the infinite-barrier jellium model in computing the s-electron contribution) and (2) a semi-empirical approach, the embedded atom method [10]. This

* Permanent address: Department of Physics, Haverford College, Haverford, PA 19041, USA.

paper makes no attempt to compare the relative utility of these state-of-the art approaches. However, Muscat has applied his method most broadly, studying hydrogen – the easiest adsorbate to treat in these approaches – on a variety of late transitions metal faces [6–9]. To assess the accuracy of the energies obtained, one can compare the phase diagram predicted by a set of interaction energies with that measured by experiment (typically LEED).

Earlier embedded cluster calculations [3] generally seem to have the correct signs to predict the ordered phases [but not for H/Pd(111), where a (2×2) phase is predicted [11] but not observed] and are of the correct order of magnitude in size. However, for the case of H/Ni(111) those earlier calculations have been shown [12] to predict a maximum disordering temperature below 70 K whereas the experimental value is 270 K. While this progress is impressive, the remaining discrepancies suggest that it is premature to base further conclusions, such as choosing between structural models [13], exclusively on interactions calculated in this way.

These earlier calculations for (111) transition metal surfaces involved seven embedded spheres representing substrate atoms and only two adatoms at the appropriate spacings. Recently Muscat has published more extensive calculations [4] for H/Ni(111). The new work uses larger clusters of substrate spheres (12 and 19 atoms), allowing a more symmetrical grouping of (3 or 6) adatoms. As in other recent papers [6,7], Muscat then deduced the interactions from fits to the calculated total energies of these clusters. These improvements significantly altered the estimates for the shorter-range interactions and allowed further-range interactions to be extracted as well.

At his suggestion [14] we have undertaken Monte Carlo studies of the phase diagrams of honeycomb lattices with his refined interaction energies. While we do now find the correct ordered phase with about the right maximum transition temperature, there are important *qualitative* discrepancies between the topology of these phase diagrams and the experimental one, indicating that further study of these interaction energies is warranted. An unusual feature of Muscat's lateral interactions is that they do *not* decay with increasing separation; the shortest-range attraction is not "stabilized" by shorter, stronger repulsions. There are two possible consequences. The ordered phases induced by strong attractive interactions at the associated relatively long inter-adatom spacing may be unstable to collapse to denser phases when there are not short range repulsions. This sort of effect will be immediately obvious in LEED due to the absence of the spots distinguishing the sparser from the denser phase. Secondly, even when this collapse does not occur, the ordered phase will exist only for a small range of coverages near its saturation coverage, with large mixed-phase regions on both higher and lower coverage sides. Since the boundary between the long-range ordered and these mixed-phase regions is not obvious in LEED, this effect must be inferred from the phase boundary with the disordered region.

Our plan in this paper is first, in section 2, to set the stage by describing the H/Ni(111) system, including the experimental phase diagram and Muscat's interactions. In section 3 we bring out our essential points by recalling similar results from the simpler, classic problem of the Ising metamagnet. We illustrate these comments with transfer matrix calculations on the equivalent square lattice gas with strong second-neighbor attraction and weaker first-neighbor repulsions. In section 4 we present Monte Carlo calculations of the phase diagram generated by Muscat's interactions. For completeness, in section 5, we discuss further work bearing on the H/Ni(111) phase diagram, including refinement of a previously presented [15] phase diagram for this system. Section 6 offers a brief conclusion. Three appendices provide further discussions. Appendix A collects additional results on the Ising metamagnet, including comments on its critical point of order four, the crossover behavior associated with the nearest neighbor interaction, generalizations to a triangular lattice, and comments on why tricritical points rather than critical endpoints are expected. Appendices B and C report transfer-matrix finite-size scaling calculations for the disordering transition of two ordered states on a honeycomb lattice. In appendix B, the hard hexagon problem, i.e. nearest neighbor exclusion only, is treated with much higher precision than in previous studies. The transition, which is presumably unobservable in experiments, is shown to be Ising-like. In appendix C, the observed ordered phase [called h(2×2)] is shown to melt with 4-state-Potts-like behavior.

2. General features

The phase diagram obtained by Christmann et al. [16] is reproduced as fig. 1. The ordered phase has been identified as the 2×2 honeycomb phase, i.e. a (2×2) net with a two-atom basis [for brevity hereafter called h(2×2)]. We will treat this system as a classical lattice gas [17] defined on a honeycomb grid (see fig. 2).

Based on the total energies of several symmetric clusters of H atoms, Muscat fit to obtain the interaction energies of the pairwise bonds shown in fig. 2. Following Muscat, we denote the mth-neighbor pairwise potential by ω_m; we will also use ω_m terminology to refer to the mth-neighbor bond. Then the energy of a specific configuration of the adlayer is given by

$$H = \sum_m \omega_m \sum_{\langle ij \rangle_m} n_i n_j + \tfrac{1}{2}\Delta\Big(\sum_{i \in H} n_i - \sum_{i \in F} n_i \Big), \tag{1}$$

where n_i is the occupancy variable for each site, taking on values 0 and 1 and the notation $\langle ij \rangle_m$ denoted a mth neighbor pair of sites i and j. $F(H)$ denotes the set of fcc (hcp) binding sites. Muscat's values for the ω_m's are given in table 1, which also relates his notation for the honeycomb lattice "bonds" to

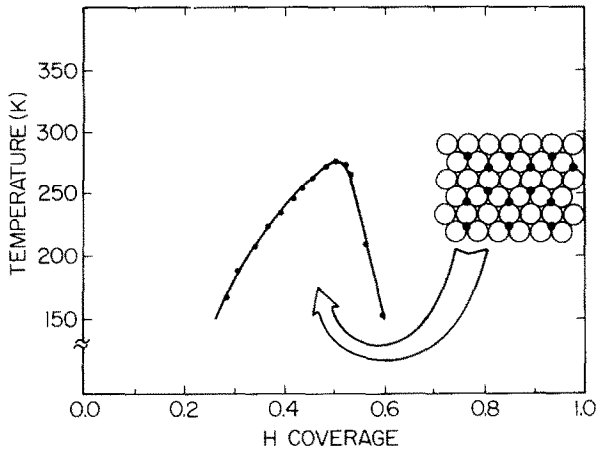

Fig. 1. Phase diagram for H/Ni(111) adapted from ref. [16]. The inset depicts the h(2×2) (graphitic) phase of H/Ni(111). The saturation coverage of this phase is 1/2 (one H atom per two Ni atoms).

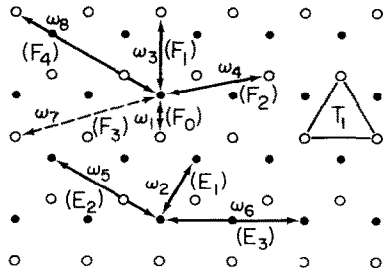

Fig. 2. Hexagonal (honeycomb) lattice of binding sites for H/Ni(111). Open circles denote hcp sites (above second layer Ni atoms) and filled circles fcc sites. There may be a small binding energy difference, Δ, between these sites. See text for discussion of bond energies.

Table 1
Sets of interaction energies for H/Ni(111)

	ω_1 (F_0)	ω_2 (E_1)	ω_3 (F_1)	ω_4 (F_2)	ω_5 (E_2)	ω_6 (E_3)	ω_7 (F_3)	ω_8 (F_4)	Δ
Muscat [4] (large, symmetric cluster)									
$d = 0$	[400]	1.5	−6.0	0.7	0.7	−18.1	–	[−4.9]	[< 20]
$d = 0.2$	[220]	6.4	−4.5	0.6	0.5	−15.0	–	[−3.6]	[< 20]
Muscat [3] (small cluster)									
$d = 0$	[450]	2	−9	–	–	–	–	–	–
$d = 0.25$	∞	−2	−9	–	–	–	–	–	–
Roelofs [15] (set VIII)	∞	1	0.2	0.2	0.2	−0.2	–	–	0.05
Nagai [41] (set III)	∞	1	0.4	0.8	0.1	−0.02	–	–	0

Muscat's numbers are in meV; the other two are in units such that $\omega_2 = 1$; ω_m refers to the mth neighbor interaction while Δ is the binding energy difference between the two kinds of three-fold sites. The notation in parentheses was used in our previous work on honeycombs to distinguish between pairs of adatoms on the same or opposite types of sites. Muscat's numbers in brackets were set to ∞ or 0 in our computations.

ours [15] for O/Ni(111). Note that our F_m's refer to pairs of adsorbates on different binding sites (one on fcc, the other on hcp) while E_m's refer to both on the same kind of site; as in our work, Muscat assumes that E_m is the same for equally separated pairs on fcc sites as on hcp sites, which is in fact the case in single-band tight-binding models [18]. Muscat's calculations were done for four values of his only adjustable parameter d, the distance from the center of the sphere for the hydrogen atom to the jellium edge. We have used his values [4] for the choices $d = 0$ and $d = 0.2$ au.

Lattice gas Hamiltonians for chemisorbed atoms should at least in principle also include multisite terms. At least in tight-binding models, one can estimate the magnitude of these terms in comparison with the pairs [19]. The issue of which to include, particularly when relatively long-range pair interactions are significant, is subtle and important. For computing phase diagrams, the smallest-perimeter triangular configuration expected to contribute is shown as T_1 in fig. 2; "shorter" trios with ω_1 legs are probably appreciable in magnitude but occur rarely because of the large ω_1 repulsion. (In our approximation, $\omega_1 = \infty$, they will never occur.) The most potent effect of multisite interactions is to introduce new ordered phases or to break lattice gas symmetries. [Cf. studies of H/Fe(110) [6,20] (but see ref. [13]), O/W(110) [19,21], and H/Pd(100) [22].] For H/Ni(111), phase diagrams consistent with experiment can be obtained with just pair interactions. Trios and higher order interactions also, of course, simply shift phase boundaries. Such effects are clearly vital if quantitative results are to be achieved, but they entail greater expenditure of computer time and lead to burgeoning parameter space. For H/Ni(111), no explicit calculations of trio energies were immediately available, but Muscat [4,6] claims that the lateral interaction energies of multi-adatom clusters are in "excellent agreement" with just the sum of the pair energies. We restricted our calculations to pairwise energies, as in eq. (1). N.B. a problem arises whenever one deduces lateral interactions from *differences* in *total* energies of various groupings of adatoms or of several sorts of ordered (not necessarily in physically observed patterns) overlayers in slab calculations. Phase boundaries are determined by excitation energies (and so differences between ordered and disordered states). Therefore the interaction energies from fits to symmetric clusters or ordered overlayers may lead to discrepancies because of the different ways in which neglected interactions cause changes in the effective values of the included interactions.

We (and Muscat [14]) suspect that his [4] relatively large value of ω_8 may be an artifact of the pairwise-interaction fit; we omit it, as does Muscat in later work. (Its size, however, might engender worries about the included couplings.) It does not introduce any new ordered states.

The interesting general feature of this set of interactions, to which we alluded above, is the relatively long range strong attraction energy $\omega_6(E_3)$. This attraction clearly lowers the energy of the p(2 × 2) phase compared to the

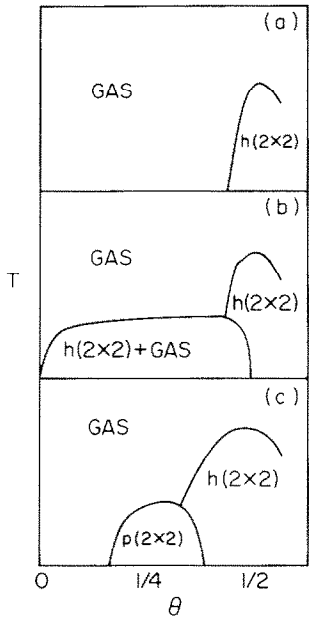

Fig. 3. Schematic "expected" phase diagrams for (2×2) honeycomb phases on an hexagonal lattice: (a), (b) two cases possible with no p(2×2) phase; (c) including a [low temperature], unseen to date p(2×2) phase.

disordered phase, but because of the ω_3 attraction, other phases have even lower energy. Of relevance here are the p(2 × 2), h(2 × 2), and p(1 × 1), with energies per adatom of $3\omega_6(E_3)$, $\frac{3}{2}\omega_3(F_1) + 3\omega_6(E_3)$, and $3\omega_2(E_1) + 3\omega_5(E_2) + 3\omega_6(E_3)$. Notice that all three phases have the same strong attractive ω_6 component. Since ω_3 is negative, the p(2 × 2) has higher per-particle energy at coverages below a half than (islands of) h(2 × 2). Since islands of h(2 × 2) will have at least the entropy of an equivalent coverage of the less dense p(2 × 2), no p(2 × 2) phase should exist. For simplicity we replace the strongly repulsive ω_1 by an exclusion, thereby precluding coverages above 1. The importance of this point is summarized below. We defer the computations and actual phase diagram to sections 4 and 5. The experimental phase diagram, however, suggests an unobserved low-temperature p(2 × 2) phase: figs. 3a and 3b give schematic temperature–coverage phase diagrams one might expect if no p(2 × 2) phase occurs. Either one should have disorder at a coverage (fig. 3a) not much less than $\theta = 0.5$ if ω_5 is repulsive, or one should have a coexistence phase of islands of h(2 × 2) and a low intensity disordered phase (fig. 3b) if ω_5 is attractive. Neither case resembles experiment, which is more consistent with fig. 3c, which includes a p(2 × 2) phase probably at a temperature below the lower limit attained in the experiment.

3. Stability of a c(2 × 2) square lattice phase

If ω_3 were repulsive instead of attractive, a p(2 × 2) phase would exist at coverages around 1/4. At zero temperature negative ω_3 causes this phase to vanish into a region of h(2 × 2) and gas coexistence. In Muscat's interaction set the ω_6 bond, which is fully saturated in the p(2 × 2) ordered state, is much larger than ω_3 and the other interaction energies. Thus at temperatures large compared to ω_3 but small compared to ω_6, one still might expect to see p(2 × 2) diffraction features at a coverage of 1/4. In order to put these questions in a more general context and to enhance physical insight, we first consider a case with fewer complications: the simple square lattice gas with nn(E_1) and nnn(E_2) interactions as shown in fig. 4:

$$H_s = E_1 \sum_{\langle ij \rangle_1} n_i n_j + E_2 \sum_{\langle ij \rangle_2} n_i n_j. \tag{2}$$

This is the lattice gas equivalent of the venerable Ising metamagnet problem [23–27]: a square lattice Ising model with antiferromagnetic nearest neighbor interaction and second neighbor ferromagnetic interaction. When $E_2 < 0$ (attractive) and $E_1 > 0$ there is a coexistence region at low temperatures between a dense c(2 × 2) phase (fig. 5) and a dilute disordered phase. If $E_1 < 0$ there is no c(2 × 2) phase. We show below that the temperature where the coexistence region vanishes is determined by the attraction, E_2 and independent of E_1, as expected, but that the disordering temperature of the c(2 × 2) phase for small E_1 is not on the order of E_1, contrary to expectation. The phase diagrams for small E_1 have distinctive features which appear in those we generate for H/Ni(111).

We have studied the phase diagram of the Hamiltonian in eq. (2) using transfer matrix finite size scaling, which has been described in several places [28,29]. The method allows fast and accurate calculation of phase diagrams and critical exponents in the case of short range interactions and reasonably dense ordered phases. It has been quite successful (i.e. rapidly convergent) for

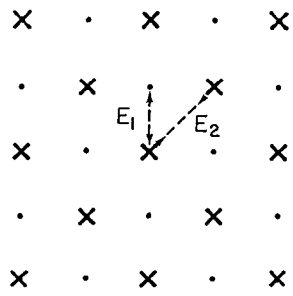

Fig. 4. c(2×2) phase in square lattice gas, with nearest and next nearest neighbor interactions indicated.

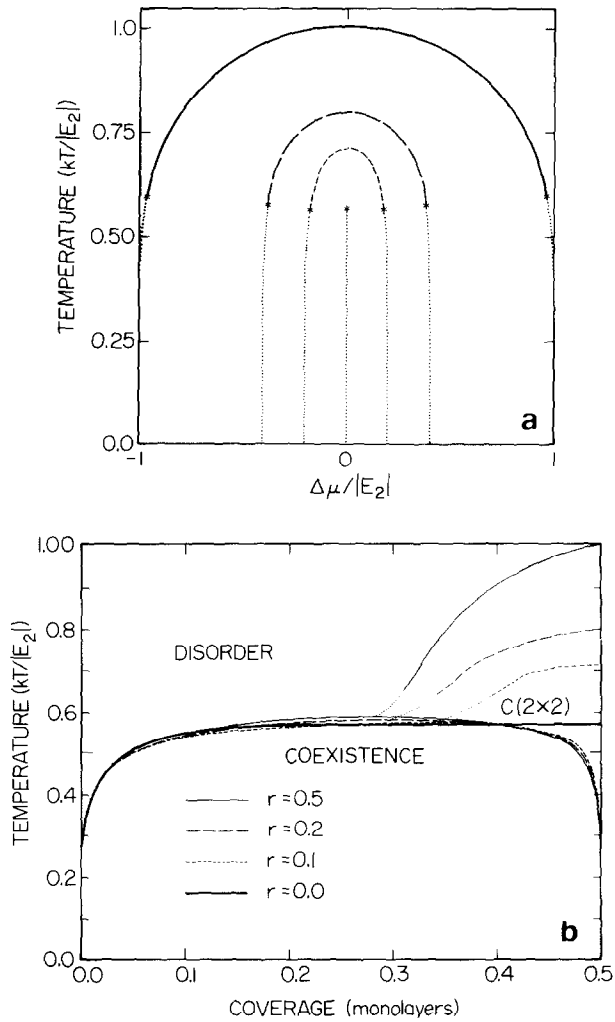

Fig. 5. (a) Temperature–chemical potential phase diagrams for the lattice gas system defined by eq. (2). Heavy lines denote second-order Ising transitions, light dotted lines are first-order transitions. The region inside the phase boundary (which vanishes in the limit $r \to 0$) is of c(2×2) character. (b) Temperature–coverage phase diagrams for the same cases as in (a). For $1/2 < \theta < 1$, the figure would be symmetric about $\theta = 1/2$. In the three cases with $r > 0$, there is a pure (i.e. long-range ordered) c(2×2) wedge-shaped region (bisected by the heavy solid line) bounded above by a second-order line and below by a first-order boundary with the coexistence region. The light dotted segment just above each tricritical point is sketched rather than computed. In the limit $r = 0$, the pure c(2×2) region has shrunk to a line at $\theta = 1/2$.

treating models with Ising critical behavior [28]. Computation of the phase boundary at temperatures below the tricritical point goes beyond routine transfer matrix scaling procedures. We developed a generalization of Hamer's method [30], which we describe elsewhere [31].

The temperature versus chemical potential phase diagrams for various values of $r \equiv -E_1/E_2$ are shown in fig. 5a. The region inside the phase boundary has c(2 × 2) symmetry. Outside this region is a disordered phase, dilute to the left and dense to the right. At both its ends the second-order Ising-like line joins a first order line at tricritical points. (See appendix A for further discussion.) As r goes to zero the c(2 × 2) phase becomes unstable with respect to segregation into dense (1 × 1) and dilute gas coexistence. The energy per atom of the (1 × 1), $2E_1 + 2E_2$, approaches that of the c(2 × 2), $2E_2$; entropy favors the collapse. One sees this decrease in stability in fig. 5 in the shrinking of the c(2 × 2) region as r gets smaller. When $r = 0$ we have a standard first-order liquid-gas type phase transition, just as one would have for the case of nearest-neighbor attractions only. The two tricritical points which occur for $r > 0$ merge to form an Ising critical point, which terminates the line of first-order transitions.

The $r = 0$ limit is also intriguing when the phase diagram is viewed in the temperature–coverage plane, where the first-order lines open into broad coexistence regions, as shown in fig. 5b. We have displayed the phase diagrams only for $\theta < 0.5$; the diagram for $0.5 \leqslant \theta \leqslant 1.0$ is a mirror image of the part shown. Only the narrow wedge near $\theta = 0.5$ (for $r > 0$) is a pure c(2 × 2) phase. The large low-temperature region is the mixed phase coexistence between c(2 × 2) and dilute gas. For $r = 0$ this pure phase has disappeared entirely and at first glance one would suppose that the coexistence changes character to become a mixture of dilute gas and dense (1 × 1), since these are the two phases on either side of the phase boundary. The situation is, however, more subtle. When $r = 0$, $E_1 = 0$, so that the system really consist of two noninteracting, interpenetrating, Ising-type lattice gas systems. Hence the critical point occurs at the Ising temperature, $kT_c/|E_2| \cong 0.567$ and the limiting curve (heavy trace) is given by the Onsager–Yang formula

$$\tfrac{1}{2} - \theta = \tfrac{1}{2}\left[1 - \sinh^{-4}(E_2/2kT)\right]^{1/8}.$$

See appendix A for a discussion of the critical behavior near $r = 0$. At $r = 0$ we have simultaneous "gas–liquid" coexistence separately on the two interpenetrating sublattices, where the dense or liquid phase on either sublattice corresponds to a c(2 × 2) phase on the full lattice. Since the two sublattices do not interact, their coexistence behavior is uncorrelated, and so they overlap in a merely statistical fashion. For example, near $\theta = 0.5$, in equilibrium, we can expect about 1/4 of the lattice to contain the dense phase on both sublattices and thus have dense (1 × 1) overall character; another 1/4 of the surface will contain the dilute phase on both sublattices and thus will have dilute gas

overall character; and the remaining 1/2 will be divided between c(2 × 2) on the two sublattices. More generally the fractions of the surfaces exhibiting the above characters are respectively θ^2, $(1-\theta)^2$ and $2\theta(1-\theta)$. In this context it is worth mentioning that in a LEED study, presuming that equilibrium has been obtained at least to the extent that the size of the islands is comparable to or greater than the resolution of the instrument, one would still see sharp c(2 × 2) beams throughout the coexistence regions in fig. 5b (except near the critical temperature where they would no longer be sharp) [32]. These beams would be arising of course from the $2\theta(1-\theta)$ fraction of the surface containing c(2 × 2) order on one or the other sublattice, while the remaining area would contribute only to scattering near integer beams. Thus the kinematic c(2 × 2) intensity in crossing the coexistence region at low temperature would be proportional to $2\theta(1-\theta)$.

For $kT \gg |E_1|$ (but below $kT_c \propto E_2$) we still expect to see this sort of behavior with a probe of finite resolution. With small negative E_1, the c(2 × 2) LEED intensity would decrease because the two sublattices are attractively coupled. Similar behavior is expected in any system dominated by (unfrustrated) long-range attraction. In the honeycomb lattice gas, the role of E_1 is played by ω_3 (but with the dense phase having h(2 × 2) order).

This difference in the character of the coexistence has less obvious ramifications for the H/Ni(111) phase diagrams because the p(2 × 2) and h(2 × 2) phases have the same set of diffraction beams. Kinematically there is a difference in intensity between the first and the second circle of half-order diffraction beams for the h(2 × 2) phase but no difference for the p(2 × 2) phase. However, multiple scattering would probably frustrate an attempt to distinguish these phases in a real experiment.

The above discussion of square lattice analogies is meant to clarify the manner in which phases disappear from phase diagrams when not stabilized by sufficiently strong shorter-range repulsions. The critical behavior of these square lattices is also interesting in its own right; some of our other observations have been collected in appendix A. We turn now to the phase diagrams we have calculated from models for H/Ni(111).

4. Phase diagrams

The phase diagram for eq. (1), with the choices for ω as given in the first row of table 1, is shown as fig. 6. We obtained this phase diagram via a Monte Carlo simulation of a hexagonal shaped lattice gas of honeycomb symmetry containing 7776 adsorption sites, a size chosen to be typical of the best metallic surfaces that can be prepared with standard methods. The runs were typically 5000 Monte Carlo steps per site, with the first 1000 discarded to allow for equilibration. As discussed in section 2, we took $\omega_8 = 0$; and since ω_1

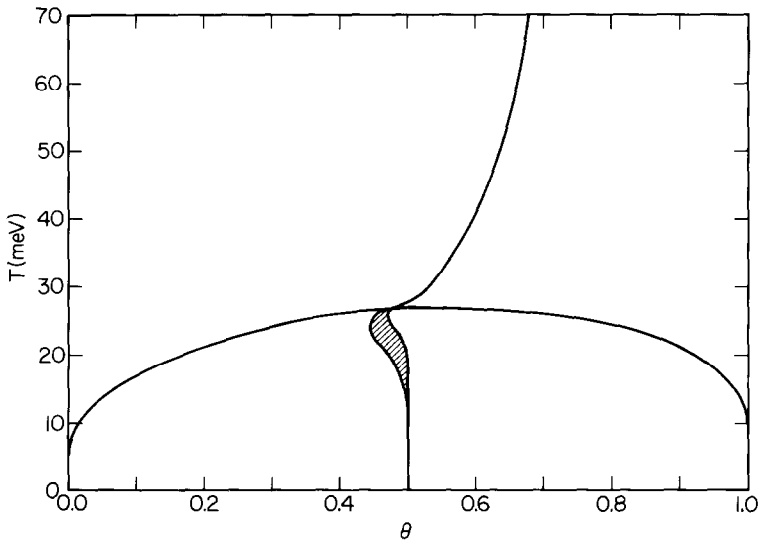

Fig. 6. Temperature–coverage phase diagram for the hexagonal lattice gas with Muscat's interaction energies for $d = 0$ given in table 1. Only the thin shaded region contains a long-range ordered h(2×2) phase. All lines are first-order except the high-temperature gas-p(1×1) line. Accurate depiction of the region near $\theta = 1/2$, $T = 27$ meV$/k$ would require much more careful study than undertaken (or warranted) in our calculations.

is very repulsive, we replaced it by an exclusion. Since Muscat [9] (also footnote 6 of ref. [4]) finds that Δ is exceptionally small for Ni, we set it to zero. In section 5 we discuss in the context of a different set of interactions the sort of changes found in a phase diagram when Δ is small but non-vanishing.

Consistent with our comments in section 2 and in analogy to the square lattice results of section 3, we see that no p(2 × 2) phase exists near $\theta \approx 0.25$. Instead, the system collapses into a coexistence of a dilute disordered phase [of (1 × 1) symmetry] and h(2 × 2). Above $\theta = 0.5$ one has a coexistence of h(2 × 2) and a (1 × 1) phase. A pure h(2 × 2) phase exists for a small coverage range around $\theta = 0.5$. The melting of this phase is expected to be in the 4-state Potts universality class; in appendix C we present transfer matrix calculations supporting this assignment. We note that the only phase seen in the experiment is reproduced by this interaction set. The maximum transition temperature of this phase is also in approximate accord with experiment, $T_c^{max} \cong 27$ meV (~ 313 K). Note that, from the discussion in appendix A, if only ω_6 were present then $T_c^{max} \sim 0.91 \mid \omega_6 \mid \sim 16$ meV; this is raised considerably by ω_3 and slightly by the others. However, the shape of the region in the T–θ plane is quite different in the two cases, indicating that some changes are needed in the interaction set. As corroboration of our phase diagram in fig. 6, an isotherm calculated at $T = 20$ meV is displayed in fig. 7. When the chemical potential is

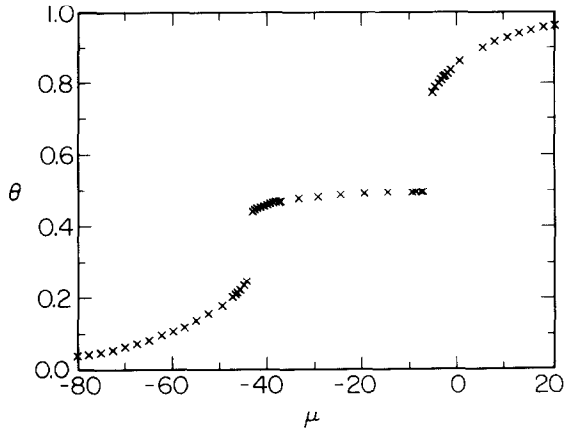

Fig. 7. Isotherm at $T = 20$ meV$/k$ for the interaction energies used in fig. 6.

fixed, the coverage ranges of the coexistence regions are thermodynamically inaccessible. These ranges, given in fig. 6, are seen as the coverage jumps in fig. 7, which occur at the values of the chemical potential on the first order lines at $T = 20$ meV in a T–μ version of fig. 6.

We note further that the calculated phase diagram contains another phase transition at higher temperatures, from a dilute phase with hexagonal symmetry (both fcc and hcp sites occupied) to a dense p(1 × 1) phase with only one type of site occupied. This transition continues to high temperature and is believed to be Ising in that limit (hard hexagons on a honeycomb, where $\theta_c = 0.829$). Transfer matrix calculations to corroborate this classification are presented in appendix B. In our calculations, transitions along this line appear to be continuous all the way down to where it joins the h(2 × 2) phase boundaries. This transition, if it actually occurs in the real system, would be difficult to detect experimentally: First, its only manifestation would be intensity variation and some critical scattering in the vicinity of some of the integer beams. Second, the H scattering is very weak compared to that of the Ni substrate [16]. Hence the only hope to see the transition is at a LEED voltage such that the clean-substrate [10] or [01] beam intensity is very weak (especially near a minimum of the I–V profile). If we let Δ be finite, the low coverage phase will also have weak p(1 × 1) symmetry and the actual phase transition will be destroyed. For small Δ, however, a deviation from $\Delta = 0$ behavior will occur only close to the transition.

In fig. 6 (and in fig. 9, to be discussed shortly) we have drawn the high-temperature line to intersect the highest temperature of the h(2 × 2) region, reminiscent of fig. 5. Monte Carlo simulations (and any experiment) are problematic near the intersection point. There is no basis to exclude the

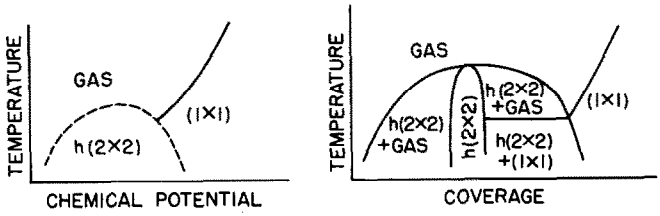

Fig. 8. Sketch of a phase diagram if the gas-(1×1) line does not intersect the $h(2\times2)$ at its peak. (a) Temperature versus chemical potential; the dashed line is first-order while the solid line is second-order. (b) Same system in temperature versus coverage.

possibility that the high-temperature line intersects below the peak, at a critical end point, as sketched in fig. 8. In this case there would be a small wedge-shaped $h(2\times2)$ + gas phase on the high-coverage side of the long-range $h(2\times2)$ phase.

In fig. 9 we show the phase diagram for Muscat's $d = 0.2$ au set. From table 1, we note that the most significant change is the quadrupling of the $\omega_2(E_1)$ repulsion. In comparing fig. 9 with fig. 6, the most noticeable change is in the high-coverage side of the $h(2\times2)$ phase: the increased ω_2 suppresses the $p(1\times1)$ phase, making the boundary nearly vertical. Similarly, the high temperature transition from the gas to the $p(1\times1)$ phase is shifted to higher coverage. Unfortunately, as noted above, this line, which would provide a good gauge of ω_2, is not readily seen experimentally. The transition from the

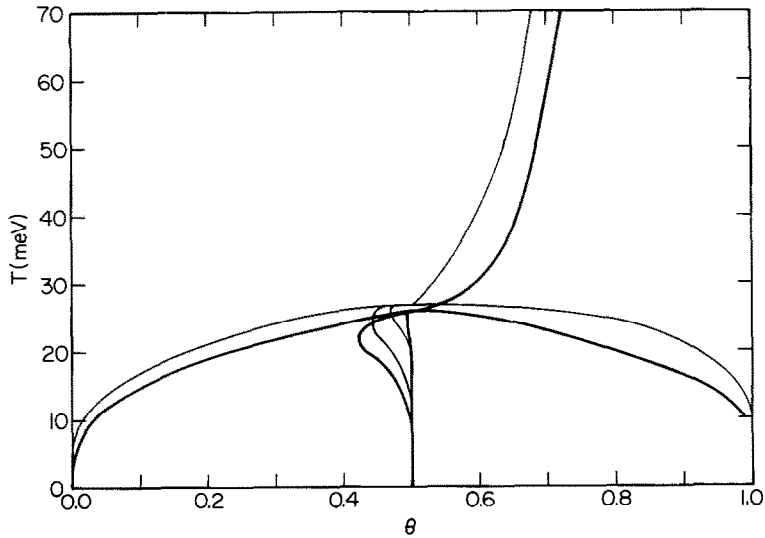

Fig. 9. Temperature–coverage phase diagram for Muscat's interaction energies for $d = 0.2$ au (thick lines). For ease of comparison, the phase boundaries from fig. 6 are reproduced (thin lines).

mixed phases is suppressed in temperature, consistent with the decrease of the energy needed to excite from h(2 × 2) ordering (due to the decrease in the attractions responsible for the ordered phases).

5. Other interaction sets

It is not hard to produce a set of interaction energies that will yield a phase diagram the high-temperature part of which will be consistent with experiment. The details of the low-temperature part – for which we have no experimental information – are sensitive to the competition between the several interactions. Hence, rather than producing several types of such consistent diagrams, we restrict ourselves to discussing two treatments in the literature. Both calculations used similar parameters in that (1) ω_6 is the only attractive interaction, (2) $|\omega_6|$ is smaller than the shorter-range repulsions, and (3) nearest-neighbor exclusion ($\omega_1 = \infty$) is assumed.

The first calculation, by one of us [15] relied on Monte Carlo. We have refined this study somewhat with larger lattices (1944-site hexagonal, as above, rather than 1152-site rhombohedral), and some longer runs at intermediate temperatures, where we have looked more closely at this unmeasured region. The temperature versus coverage phase diagram is sketched in fig. 10. The inset shows the corresponding temperature–chemical potential phase; as in fig. 9, this experimentally less accessible plot is simpler to grasp. All solid lines are first-order transitions. The higher-coverage, low-temperature coexistence phase, corresponding to the short interior solid line in the inset, was not previously noted [15]. If Δ were zero, as in the other interaction sets considered, then the phases labeled *(2×2)* would be h(2 × 2). In this case, the thin dotted line in the inset would be a critical line rising from a tricritical point to join the "outer" boundary at a critical end point. Since Δ is finite, the *(2×2)* is a (higher-density) p(2 × 2) phase, with the fcc sites preferentially occupied. As for the gas-p(1 × 1) line, the finite Δ destroys the second-order transition (leaving only a critical point at the top), since the "honeycomb" phase develops p(2 × 2) symmetry; nonetheless we find broad, weak peaking of the specific heat in the region near the line. Above the saturation coverage, the decline in transition temperature is not so precipitous as we originally concluded. Particularly careful and long runs are needed here since disordering from the honeycomb requires a two-step process. We studied the high-temperature region to see whether the transition might be continuous rather than first-order. Histograms of a 10000 MCS run at $\mu = 0.79$, $T = 0.6$ showed a two-peak order parameter distribution. While this behavior can sometimes occur at second-order transitions [33–35] one would expect the peaks to move together with increasing lattice size [34]. For a 15000 MCS run on a smaller 864-site hexagonal lattice, we did not see the peaks separate significantly,

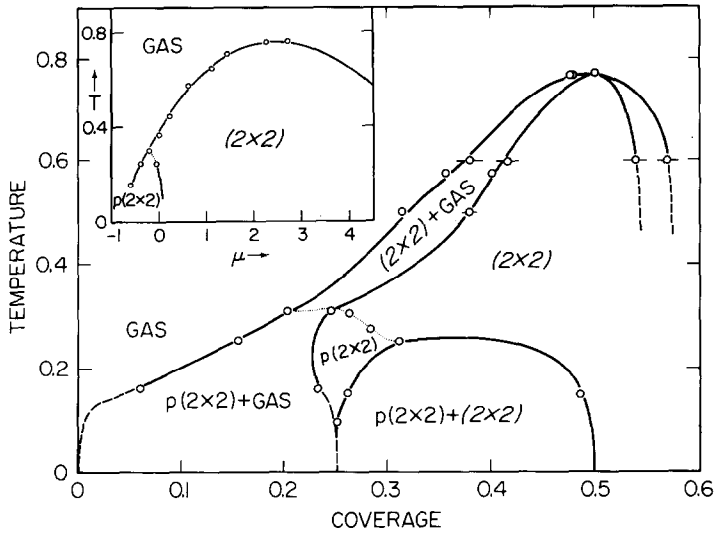

Fig. 10. Temperature–coverage phase diagram for interaction energies of Roelofs's set VIII described in table 1. Inset depicts the chemical potential versus temperature phase diagram. All solid lines are first-order. The dotted lines suggest remnants of a continuous transition destroyed by the finite Δ. The label *(2×2)* denotes h(2×2) when $\Delta = 0$ and p(2×2) when Δ is finite. See text for discussion.

consistent with the original designation. The only way to be certain about the order of the transition is to perform exhaustive calculations for several lattice sizes [36]. We also studied the high-coverage side at this temperature for $\mu \lesssim 4.4$. Two-peaked order parameter distributions were again found sometimes. We faced the added complication of slow dynamics noted above. A clear resolution would have required very long runs, possibly aided by a continuous-time method [37]. While we may carry out more extensive computations in the future, our goal here is to explore how calculations can be used to elucidate experimental data, for which rigorous finite-size studies are rarely, if ever, an option. Instead, it is more relevant to see what information can be gleaned from a lattice of size comparable to the plateau size or typical defect-free area of the actual sample. For example, fig. 11 shows a plot of the intensity at the center of the outer half-order spot versus coverage for $kT = 0.6 \times \omega_2$, about 3/4 of the maximum T_c. Since this intensity is an order parameter squared [38], we expected that in an infinite system the curve is concave down until it vanishes for a second-order phase transition. In a finite system, rounding develops when the correlation length becomes comparable to the system size; the resultant point of inflection provides an estimate of the critical coverage [39]. In fig. 11 we observe instead a broad change from concave down to concave up, consistent with our conclusion that the transi-

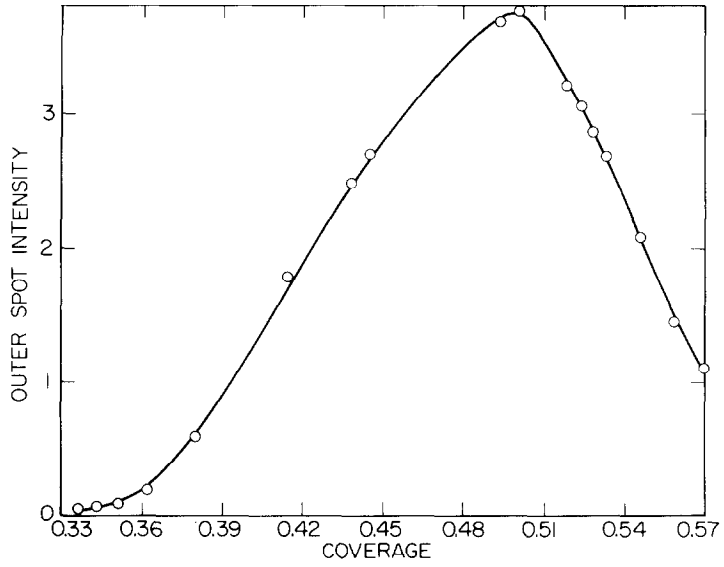

Fig. 11. Plot of intensity (small circles) of the outer half-order becomes coverage computed at $T = 0.6\ \omega_2/k$. This sort of plot might be measured (cf. fig. 2 of ref. [16]).

tion of this interaction set is first-order. (A mixed phase region is manifested on such a plot by a region of quadratic dependence of I on $(\theta - \theta_0)$, where θ_0 is the coverage of the disordered phase near the transition. Very long runs would be needed to characterize the dependence of I on θ with confidence, but the gradual variation of curvature suggests that both transitions – below and above saturation coverage – are first-order.) If an experimentalist measures the *integrated* spot intensity near a second-order transition, one expects an energy-like anomaly [39], i.e. const. $\pm |\theta - \theta_c|^{1-\tilde{\alpha}}$ – the tilde is a reminder that the specific heat exponent must be Fisher renormalized [40]: $\tilde{\alpha} \equiv -\alpha/(1 - \alpha)$. Hence, unless the transition is Ising-like, there will be no sharp anomaly even for a second-order transition. Consistent with this discussion, in fig. 2 of ref. [16] (at half the maximum T_c) nothing remarkable happens at the critical coverages.

Nagai et al. [41] analyzed a rather similar set of interactions and produced phase diagrams that would be similar to fig. 10 if the high-temperature boundary were a continuous transition. The first version [41a] would then be topologically essentially identical to ours, although they take no note of the experimentally elusive high-temperature continuous transition between gas and (1×1) that should be present for their interactions, since $\Delta = 0$. [The $p(2 \times 2)$ to $h(2 \times 2)$ continuous transition is observed.] Curiously, a later detailed exposition [41b] does not mention this earlier letter but omits the high-coverage tricritical point that ushers in the mixed $h(2 \times 2)$–(1×1) phase

as well as the lower-coverage, lower-temperature one associated with the mixed p(2 × 2)–h(2 × 2) region. These phase diagrams were constructed using the method of Berker and co-workers [42]: a prefacing transformation followed by Migdal–Kadanoff real space renormalization. While this procedure is a powerful and elegant way to survey parameter space, our experience in comparisons on square lattices [43] has suggested that quantitative predictions should be checked. In the present case we computed with Monte Carlo the highest-T critical point, which occurs at $T = 0.58$ ($\mu = 3.8$), compared with $T = 0.40$ ($\mu = 3.1$) in Nagai et al. [41].

6. Conclusion

Impressive progress has been made in the calculation of electronic indirect interactions between chemisorbed atoms. Rather than describing general trends, one can now make predictions about some specific systems. Muscat's embedded cluster calculations generally yield estimates of hydrogen–hydrogen interactions that have the correct sign, give the correct ordered phases, and predict the (maximum) transition temperature to within better than an order of magnitude. This advance challenges us to determine lateral interactions more precisely from fits to experimental data, especially phase diagrams, and conversely to check how well the calculated interactions reproduce such phase diagrams. In order to achieve "excellent agreement" with the experiment, the interactions should lead to the correct topology of the phase diagram. In this paper we have shown that for H/Ni(111), Muscat's interaction energies give large coexistence regions at high and low coverages which are not seen experimentally. The main cause of this discrepancy is the comparatively (and surprisingly) large ω_6 attraction. By considering the simpler Ising metamagnet, we have shown that these large coexistence regions are characteristic of long-range attractions unsupported by shorter-range repulsions. We thus conclude that the strong ω_6 attraction probably does not occur in the real H/Ni(111) system.

To actually determine with any confidence (say to within a factor of two) values of the adatom–adatom interactions from the known H/Ni(111) phase diagram is impossible. There are simply too many interactions that could conceivable be important but have similar effects on the phase diagram. (For example trio interactions are probably not negligible for H/Ni(111) but their effects on the phase diagram are hard to distinguish from pair interactions because they break no lattice gas symmetries.) Nevertheless we have presented refined calculations on an interaction set which has a phase diagram more in accord with experiment. To be more confident about this type of interaction set, more information is needed: principally whether there is a low-temperature p(2 × 2) phase. Occurrence of a phase transition between the disordered

phase and the (1×1) phase at high temperatures near a coverage of 0.83 would confirm Muscat's prediction that the binding energy difference between the fcc and hcp sites is small; observation of it, however, presents a major experimental challenge.

Acknowledgements

We thank J.-P. Muscat for prompting us to (re-)consider this system and for helpful correspondence and a preprint of ref. [9]. We also thank A.L. Stella and S. Fishman for useful comments. This work was supported by Department of Energy Grant No. DE-FG05-84ER-45071. Computer facilities were supplied in part by the University of Maryland Computer Science Center. During the final stage of this work one of us (TLE) gratefully acknowledges the hospitality of the Surface Science Division of the National Bureau of Standards and its support under an Intergovernmental Personnel Act assignment. Another of us (LDR) gratefully acknowledges partial support by the Alexander von Humboldt Foundation and the hospitality of the Fritz Haber Institute of the Max Planck Society and of the Institute for Physical Chemistry of the University of Munich.

Appendix A

In this appendix we collect several remarks pertinent to the Ising metamagnet. While related to the discussion in the text, exposition there would have distracted from the thread of our arguments. In the Ising metamagnet the special point at $E_1 = 0$ (or $r = 0$) and $\mu = 0$ (or $\theta = 1/2$) has received considerable attention. At this point, when (in an extended parameter space) both the "magnetic field" (i.e. μ) and the staggered field (possible binding energy difference between the two c(2×2) sublattices) vanish, we find a critical point of order four, where two tricritical lines meet [25,44]. In renormalization group [27], this point is a (sublattice) ferromagnetic fixed point, called SF. At this point, the two sublattices decouple into two simple Ising (lattice gas) models with nearest neighbor attraction E_2. Thus, as illustrated in fig. 5, $kT_c/E_2 \cong 0.567$, a long-known result [23].

It is not hard to show that the crossover exponent associated with the field E_1 is $2 - \alpha = 2$: Writing $f \propto t^{2-\alpha} X(E_1/t^{\phi})$, we note

$$\left.\frac{\partial f}{\partial E_1}\right|_{E_1=0} \propto t^{2-\alpha-\phi}\, X'(0).$$

But this derivative is just the nearest neighbor correlation function. At $E_1 = 0$ the two sublattices are decoupled, making this correlation function constant,

so that $2 - \alpha - \phi = 0$. Since this special point is Ising-like, $\alpha = 0$. Thus $T_c(E_1) - T_c(E_1 = 0) \propto E_1^{1/2}$ for small E_1 [45]. Fig. 5 is consistent with this result.

Recall also for the metamagnet that the free energy is symmetric in the sign of the nearest neighbor exchange interaction; the change of sign is accomplished by a simple inversion of one of the two sublattices. While in the lattice gas one would also have to adjust the chemical potential target to get a symmetry, we do learn that if E_1 becomes attractive, we go over to a (1×1) Ising situation and $T_c(E_1) - T_c(0)$ is still proportional to $|E_1|^{1/2}$ [46]. Similarly, on a triangular lattice with (strong) attractive second neighbor interaction E_2, the full lattice decouples into *three* sublattices. The transition temperature $T_c^{\Delta}(0)$ is given by [47] $kT_c^{\Delta}/E_2 = 1/\ln 3 = 0.91\ldots$. As E_1^{Δ} is raised from zero, T_c^{Δ} again rises by $E_1^{1/2}$, but now the crossover is from Ising to 3-state Potts behavior.

We next comment on the claim of tricritical points in fig. 5. We see no evidence that the second-order line intersects either first-order line away from the latter's end, i.e. at a critical end point [48]. Moreover, real-space renormalization group studies [49] show a tricritical point at $T \gtrsim 2E_2$, nearly independent of E_1, as in these figures. Mean field calculations [26,48b] suggested that for $r > 5/3$ a critical end point should exist, but such calculations are unreliable for $2D$ phase boundaries; Huse's [50] interpretation of Baxter's exact solution indicates the existence of a tricritical point for $r = \infty$.

Finally we note that a square lattice analogue even more germane to H/Ni(111) is an extension of eq. (2) to include a third neighbor interaction, with E_3 being strongly attractive, E_2 attractive but weak, and E_1 weakly repulsive. For $E_1 = 0 = E_2$ the lattice again decouples into *four* square $p(2 \times 2)$ Ising sublattices. As E_2 becomes negative, the $p(2 \times 2)$ coexisting phases collapse into two Ising $c(2 \times 2)$ sublattices and T_c rises by $|E_2|^{1/2}$. When E_1 becomes positive, the $c(2 \times 2)$ character persists and T_c rises further by $E_1^{1/2}$.

Appendix B

To estimate the critical point of the honeycomb lattice gas with only nearest neighbor exclusions we used the standard technique of applying finite size scaling theory to the properties of lattice gases on the surfaces of infinitely long cylinders. We used transfer matrix techniques to compute the correlation length ξ and coverage θ of these systems, and then the critical activity z, correlation length exponent ν, and anomalous dimension exponent η. While this problem has been studied before by similar techniques [51], our estimates of z_c and θ_c are three orders of magnitude more accurate because we could attain larger strip widths via sparse matrix decomposition [28b,52] of the transfer matrix. (Our first entry in table 2 is the final entry of ref. [51].)

Table 2
List of estimates of critical activity, correlation length exponent, anomalous dimension, and critical coverage based on eqs. (B.3), (B.4), (B.5) and (B.2), respectively

L	$\tilde{z}_c(L)$	$\tilde{\nu}(L)$	$\tilde{\eta}(L)$	$\tilde{\theta}(z_c^{ex}, L)$
8	7.828031282	0.9982027	0.2539521	0.82933162
9	7.835503782	0.9988421	0.2530325	0.83932721
10	7.840112737	0.9992201	0.2524038	0.82932461
11	7.843117968	0.9994564	0.2519538	0.82932298
12	7.845165936	0.9996121	0.2516197	0.82932190
13	7.846611718	0.9997188	0.2513644	0.82932116
14	7.847662234	0.9997948	0.2511648	0.82932064
15				0.82932027
Ex	7.85177(3)	1.00006	0.25003	0.829318(3)

Extrapolated values are listed at the bottom. The critical coverage is evaluated at the extrapolated critical activity rather than $\tilde{z}_c(L)$.

The transfer matrices were constructed so that the axis of a cylinder (i.e. the "infinite" direction) was parallel to a line drawn between two nearest neighbor sites (i.e. an ω_1 direction). The transfer matrix between rows of one triangular sublattice can be written as the product of two $2^L \times 2^L$ matrices, where L is the number of sites in one row of a sublattice in the finite direction; the first matrix transfers to the alternative sublattice, the second transfers back. The two largest eigenvalues of the transfer matrix were found by decomposing each of these matrices as a product of L sparse matrices and then applying a power method. The coverage was found by differentiating the largest eigenvalue, λ_0, with respect to activity, z ($z = \exp(\mu/kT)$):

$$\theta(z,L) = (z/L)\,\partial[\ln \lambda_0(z,L)]/\partial z. \tag{B.1}$$

The correlation length in terms of a, the nearest neighbor spacing on a triangular sublattice, is defined by

$$\xi^{-1}(z,L) = (2/\sqrt{3}\,a)\,\ln(\lambda_0/\lambda_1), \tag{B.2}$$

where the second largest eigenvalue, λ_1, is positive (and real) near the phase transition. Finite size scaling theory estimates the critical activity, z_c, by the hypothesis that the critical correlation length is proportional to L, or

$$\xi(\tilde{z}_c(L),L)/L = \xi(\tilde{z}_c(L),L+1)/(L+1). \tag{B.3}$$

Table 2 lists the critical point estimates $\tilde{z}_c(L)$ for $8 \leqslant L \leqslant 14$. The exponent ν can be estimated by

$$\left(\frac{L+1}{L}\right)^{1+1/\tilde{\nu}} = \frac{\partial\xi(\tilde{z}_c(L),L+1)/\partial z}{\partial\xi(\tilde{z}_c(L),L)/\partial z}. \tag{B.4}$$

An estimate of η is afforded by the predictions of conformal invariance [53]:

$$\tilde{\eta}(L) = aL/\pi\xi(\tilde{z}_c(L), L). \tag{B.5}$$

These estimates also appear in table 2. The transition is to high precision Ising-like ($\nu = 1$, $\eta = 1/4$). The extrapolated values of η and ν were obtained by fitting the final three entries to the form $a + bL^{-x}$. The critical activity extrapolation was obtained by applying this power law fitting procedure twice: first the $L-1$, L, and $L+1$ values of $\tilde{z}_c(L)$ were fit to $\tilde{\tilde{z}}_c(L) + bL^{-x}$ for $L = 10$, 11, 12, and 13. In turn the critical activity estimates $\tilde{\tilde{z}}_c(L)$ for $L = 11$, 12, and 13 were fit to the same form to give the extrapolation appearing in table 2. The indicated uncertainty is the difference between the results of the final fit of $\tilde{\tilde{z}}_c(L)$ using $L = 11$, 12, and 13 and the result for 10, 11, and 12. An estimate of z_c made on the basis of eq. (B.5) with η fixed at 1/4, rather than with eq. (B.3), gave essentially the same results, confirming our number of significant digits. Finally the critical coverage was estimated by computing the coverage at the best estimate of the critical activity; the uncertainty in the extrapolated result comes mostly from the uncertainty in the critical activity.

Appendix C

To try to find the critical behavior of a second order h(2 × 2)–disorder transition we studied a lattice gas model with the minimal number of interactions needed to form the h(2 × 2) ordered state: an $\omega_2(E_1)$ repulsion and an $\omega_3(F_1)$ attraction. Notice that an $\omega_2(E_1)$ repulsion alone is not sufficient to form the h(2 × 2) phase, contrary to previous claims [41b,54], because rows of h(2 × 2) could then slide with respect to each other with no cost in energy.

We estimated the exponent ν for the case $F_1 = -10E_1$ ($\theta_c \approx 0.499$) $\mu = -3.55$ using the transfer matrix scaling approach reviewed in appendix B. We chose this rather unnatural interaction set to avoid the appearance of the sliding phase described in the previous paragraph. By studying all the relevant subdominant eigenvalues we find only one phase transition: all the correlation lengths which scale linearly with system size do so at approximately the same temperature. This is not so obvious at much smaller values of $|\omega_3|$, where there is evidently, a sliding phase between the h(2 × 2) and disordered phases. The transfer matrix propagated the lattice in the same direction as the one used in appendix B. It cannot, however, be decomposed in the same way because of the longer-range interactions. Instead of transferring between rows of the same sublattice, it transferred between pairs of rows in both sublattices. We found it most convenient to find the largest eigenvalues of this matrix by reducing its size by using cyclic permutation symmetry [55] rather than by using the sparse matrix decomposition. The (2, 4), (4, 6) and (6, 8) estimates of ν are 0.732, 0.701, and 0.705, respectively. The correlation length used in these

estimates came from the largest eigenvalue whose eigenvector changed sign under cyclic permutation of the rows of the lattice; other eigenvectors gave similar results. The value of ν for the 4-state Potts model is 2/3. The observed estimates of ν, and the poor convergence, are typical of the 4-state Potts model [56]. (The poor convergence is taken as a sign of a marginal operator.)

It is also possible to investigate the critical properties of the melting of this phase using Monte Carlo finite-size scaling [57]. If a measurable $G(t)$, $t = |T - T_c|/T_c$, behaves like t^λ near T_c, then plots of $\log(L^{\lambda/\nu} G)$ versus $\log(tL^{1/\nu})$ for various T and L should lie on one universal curve for T above T_c and on a second for T below T_c. Then T_c and the exponents can be estimated by adjustment to "sharpen to focus" of the curves. Our results from a short study using this procedure are consistent with the transfer matrix results but not nearly so convincing.

References

[1] T.L. Einstein, in: Chemistry and Physics of Solid Surfaces, Vol. 2, Ed. R. Vanselow (CRC Press, Boca Raton, FL, 1979) p. 181, and references therein.

[2] J.-P. Muscat and D.M. Newns, Surface Sci. 105 (1981) 570.

[3] J.-P. Muscat, Surface Sci. 110 (1981) 85.

[4] J.-P. Muscat, Surface Sci. 152/153 (1985) 684.

[5] P. Nordlander and S. Holmström, Surface Sci. 159 (1985) 443.

[6] J.-P. Muscat, Surface Sci. 139 (1984) 491.

[7] J.-P. Muscat, Surface Sci. 148 (1984) 237.

[8] J.-P. Muscat, Progr. Surface Sci. 18 (1985) 59.

[9] J.-P. Muscat, Ordered Hydrogen Overlayers on Metal Surfaces, Phys. Rev. B33 (1986) 8136.

[10] M.S. Daw and M.I. Baskes, Phys. Rev. Letters 29 (1983) 1285; Phys. Rev. B29 (1984) 6443; S.M. Foiles and M.S. Daw, J. Vacuum Sci. Technol. A3 (1985) 1565.

[11] Ref. [9] indicates a large binding energy difference Δ for H/Pd(111) which would preclude the spurious h(2×2); however, the experimental $(\sqrt{3} \times \sqrt{3})$ still is not obtained, J.-P. Muscat, private communication, 1985.

[12] N.C. Bartelt, T.L. Einstein and L.D. Roelofs, J. Vacuum Sci. Technol. A1 (1983) 1217. For $d = -0.2$, 0, and 0.25, ref. [3] gives ratios ω_2/ω_3 of 0.385, −0.222, and 0.222, with predicted kT_c/ω_3 of 0.36, 0.64, or 0.46 or $T = 55$, 67 or 48 K, respectively.

[13] Cf. e.g. W. Moritz, R. Imbihl, R.J. Behm, G. Ertl and T. Matsushima, J. Chem. Phys. 83 (1985) 1959.

[14] J.-P. Muscat, private communication, 1985.

[15] L.D. Roelofs, in: Chemistry and Physics of Solid Surfaces, Vol. 4, Eds. R. Vanselow and R. Howe (Springer, Berlin, 1982) p. 219; Thesis, University of Maryland, 1980, unpublished.

[16] K. Christmann, R.J. Behm, G. Ertl, M.A. Van Hove and W.H. Weinberg, J. Chem. Phys. 70 (1979) 4168.

[17] It may eventually be necessary to take into account quantum corrections for H overlayers.

[18] P.E. Hunter, T.L. Einstein and L.D. Roelofs, Bull. Am. Phys. Soc. 25 (1980) 194;
L.D. Roelofs, T.L. Einstein, P.E. Hunter, A.R. Kortan, R.L. Park and R.M. Roberts, J. Vacuum Sci. Technol. 17 (1980) 231.

[19] T.L. Einstein, Surface Sci. 84 (1979) L497;
T.L. Einstein and P.E. Hunter, Bull. Am. Phys. Soc. 24 (1979) 312.

[20] W. Kinzel, W. Selke and K. Binder, Surface Sci 121 (1982) 13;
W. Selke, W. Kinzel and K. Binder, Surface Sci. 125 (1983) 74.
[21] W.Y. Ching, D.L. Huber, M.G. Lagally and G.C. Wang, Surface Sci. 77 (1978) 550.
[22] K. Binder and D.P. Landau, Surface Sci. 108 (1981) 503.
[23] C. Fan and F.Y. Wu, Phys. Rev. 179 (1969) 560.
[24] M. Plischke and D. Mattis, Phys. Rev. A3 (1971) 2092, studied the metamagnet using transfer matrices, without the benefit of finite size scaling.
[25] F. Harbus, A. Hankey, H.E. Stanley and T.S. Chang, Phys. Rev. B8 (1973) 2273.
[26] J.M. Kincaid and E.G.D. Cohen, Phys. Rept. 22 (1975) 57.
[27] J.M.J. van Leeuwen, Phys. Rev. Letters 34 (1975) 1056.
[28] M.P. Nightingale, (a) Physica 83A (1976) 561; (b) Proc. Koninkl. Ned. Akad. Wetenschap. B82 (1979) 235; (c) J. Appl. Phys. 53 (1982) 7927.
[29] M.N. Barber, in: Phase Transitions and Critical Phenomena, Vol. 8, Eds. C. Domb and J.L. Lebowitz (Academic Press, New York, 1984) p. 145.
[30] C.J. Hamer, J. Phys. A15 (1982) L675.
[31] N.C. Bartelt, T.L. Einstein and L.D. Roelofs, Phys. Rev. B34 (1986), to be published.
[32] In this situation, the intensity of the center of the half-order beams is proportional to the number of sites (or adatoms) squared. It is distinct from the situation discussed by L.D. Roelofs, Surface Sci. 111 (1981) L680, in which antiphase domains *above* T_c lead to half-order beam heights of order the number of scatterers.
[33] M.A. Novotny and D.P. Landau, Phys. Rev. B24 (1981) 1468.
[34] D.P. Landau and R.H. Swendsen, Phys. Rev. Letters 46 (1981) 1437.
[35] J. Glosli and M. Plischke, Can. J. Phys. 61 (1983) 1515.
[36] K. Binder, in: Applications of the Monte Carlo Method in Statistical Physics, Ed. K. Binder (Springer, Berlin, 1984) ch. 1; Z. Phys. B45 (1981) 503.
[37] A.B. Bortz, M.H. Kalos and J.L. Lebowitz, J. Comput. Phys. 17 (1975) 10.
[38] D.E. Taylor, E.D. Williams, R.L. Park, N.C. Bartelt and T.L. Einstein, Phys. Rev. B32 (1985) 4653.
[39] N.C. Bartelt, T.L. Einstein and L.D. Roelofs, Surface Sci. 149 (1985) L47; Phys. Rev. B32 (1985) 2993.
[40] M.E. Fisher, Phys. Rev. 176 (1968) 257.
[41] (a) K. Nagai, Surface Sci. 136 (1984) L14;
(b) K. Nagai, Y. Ohno and T. Nakamura, Phys. Rev. B30 (1984) 1461.
In both papers the coverage scale is normalized per adsorption site rather than per Ni.
[42] A.N. Berker, S. Ostlund and F.A. Putnam, Phys. Rev. B17 (1978) 3650;
S. Ostlund and A.N. Berker, Phys. Rev. B21 (1980) 5410;
R. Caflisch and A.N. Berker, Phys. Rev. B29 (1984) 1279.
[43] P. Bak, P. Kleban, W.N. Unertl, J. Ochab, G. Akinci, N.C. Bartelt and T.L. Einstein, Phys. Rev. Letters 54 (1985) 1539.
[44] A recent review is A. Aharony, in: Critical Phenomena, Ed. F.J.W. Hahne, Springer Lecture Notes in Physics 186 (Springer, Berlin, 1983) p. 210.
[45] P. Pfeuty, D. Jasnow and M.E. Fisher, Phys. Rev. B10 (1974) 2088.
[46] Contrast this to the linear regime, e.g. with large $E_1 > 0$ and small $E_2 < 0$.
N.C. Bartelt, T.L. Einstein and E.D. Williams, J. Vacuum Sci. Technol. A2 (1984) 1006;
N.C. Bartelt and T.L. Einstein, Bull. Am. Phys. Soc. 26 (1981) 289; unpublished.
[47] J. Stephenson, J. Math. Phys. 11 (1970) 420.
[48] (a) T.A.L. Ziman, D.J. Amit, G. Grinstein and C. Jayaprakash, Phys. Rev. B25 (1982) 319 do renormalization group studies in $4-\epsilon$ dimensions;
(b) H.J. Herrmann, Phys. Letters A100 (1984) 256 suggest the existence of a critical end point for $r = 50$. The flaw in his approach is discussed in ref. [31].
[49] B. Nienhuis and M. Nauenberg, Phys. Rev. B13 (1976) 2021.

[50] D.A. Huse, Phys. Rev. Letters 49 (1982) 1121.
[51] J. Debierre and L. Turban, Phys. Letters A97 (1983) 285.
[52] M.P.M. den Nijs, M.P. Nightingale and M. Schick, Phys. Rev. B26 (1982) 2490.
[53] J. Cardy, J. Phys. A17 (1984) L385.
[54] E. Domany, M. Schick and J.S. Walker, Solid State Commun. 30 (1979) 331.
[55] W. Kinzel and M. Schick, Phys. Rev. B23 (1981) 3435; 24 (1981) 324.
[56] P. Nightingale and H.W.J. Blöte, J. Phys. A15 (1982) L33.
[57] K. Binder and D.P. Landau, Phys. Rev. B21 (1980) 1941, and references therein.